

COSMOSOMAS: A Circular Scanning Instrument to Map the Sky at Centimetric Wavelengths

J. E. Gallegos¹, J. F. Macías-Pérez², C. M. Gutiérrez¹, R. Rebolo^{1,3},
R. A. Watson², R. J. Hoyland¹ and S. Fernández-Cerezo¹

¹ *Instituto de Astrofísica de Canarias, E 38200 La Laguna, Tenerife, Spain*

² *University of Manchester, Jodrell Bank Observatory, Macclesfield, Cheshire, SK 11, 9DL, UK*

³ *Consejo Superior de Investigaciones Científicas, Spain*

9 November 2018

ABSTRACT

We describe the first instrument of a Cosmic Microwave Background experiment for mapping cosmological structures on medium angular scales (the COSMOSOMAS experiment) and diffuse Galactic emission. The instrument is located at Teide Observatory (Tenerife) and is based on a circular scanning sky strategy. It consists of a 1 Hz spinning flat mirror directing the sky radiation into a 1.8 m off-axis paraboloidal antenna which focuses it on to a cryogenically cooled HEMT-based receiver operating in the frequency range 12–18 GHz. The signal is split by a set of three filters, allowing simultaneous observations at 13, 15 and 17 GHz, each with a 1 GHz bandpass. A 1° – 5° resolution sky map complete in RA and covering 20° in declination is obtained each day at these frequencies. The observations presented here correspond to the first months of operation, which have provided a map of 9000 square degrees on the sky centred at DEC = $+31^\circ$ with sensitivities of 140, 150 and 250 μK per beam area in the channels at 13, 15 and 17 GHz respectively. We discuss the design and performance of the instrument, the atmospheric effects, the reliability of the data obtained and prospects of achieving a sensitivity of 30 μK per beam in two years of operation.

Key words: cosmic microwave background – cosmology: observations – instrumentation: detectors.

1 INTRODUCTION

In recent years experiments on angular scales from several degrees to a few arc minutes have started to delineate the CMB power spectrum offering a unique approach to the study of conditions in the early history of the Universe. Current observations at large and intermediate angular scales constrain the level of normalization of the Sachs–Wolfe plateau (Bennett et al. 1996; Gutiérrez et al. 2000), and have shown the presence of the first Doppler peak (de Bernardis et al. 2000; Hanany et al. 2000; Mauskopf et al. 2000; Halverson et al. 2001). A new generation of experiments is planned to cover angular scales ranging from a few arc minutes to several degrees, these include the *MAP* and *Planck* satellite missions. These experimental efforts will potentially allow the determination of the main cosmological parameters at a level of a few per cent. To achieve this, a very accurate subtraction of foregrounds is needed. These foregrounds include synchrotron, free–free and dust emission. Recently, a fourth component has been identified (Kogut et al. 1996a,b) in the analysis of the *COBE* DMR data. The

nature of this component is controversial and has been proposed to be free–free (Mukherjee et al. 2001) or spinning dust (de Oliveira-Costa et al. 1999, 2000). Progress in the study of this elusive component will require the existence of reliable maps at frequencies in the range between 10 and 20 GHz where free–free emission is one of the dominating processes and spinning dust (Draine & Lazarian 1998) may exhibit a turn-over in its spectrum.

The goal of the COSMOSOMAS experiment presented here is to map the cosmic microwave background and Galactic diffuse emission with mean sensitivities of 30 μK per beam ($\sim 1^\circ$) in an area covering $\sim 25\%$ of the sky. This will allow a measurement of CMB fluctuations in the angular regions of the Sachs–Wolfe plateau and the first acoustic peaks. The experiment is based on a circular scanning strategy and consists of two ground-based total power receivers working at central frequencies of 10 and 15 GHz respectively with a beam size of 1° . Observations with a prototype of the COSMOSOMAS experiment operating at 10 GHz (Gallegos et al. 1998) proved that the atmospheric conditions at Teide

Observatory were suitable for CMB experiments based on a circular scanning strategy. Although the instrumental set-up is similar for both experiments, this paper concentrates on a description of the 15 GHz instrument (which hereafter we shall refer to as COSMO15), an analysis of its performance and a presentation of its first results.

After describing the instrumental set-up (Section 2), the observations and data analysis (Section 3), we analyse the instrument’s performance (Section 4) and present maps of the sky obtained with COSMO15 (Section 5).

2 THE INSTRUMENTAL SET-UP

2.1 Optical System

The COSMO15 instrument consists of a 2.5 m flat circular mirror whose normal rotates about the central axis of spin at a rate of 1 Hz and reflects the radiation from the sky into a parabolic dish. The spin axis can be tilted to change the region of sky observed. The mirror is canted at 5° relative to its spin axis to generate a circular path on the sky with a diameter of 20° . This geometrical configuration combined with the Earth’s rotation allows for complete coverage of a full declination strip once per sidereal day. The declination range covered is given by

$$\delta_o + \beta - 2\alpha - 2\gamma \leq \delta \leq \delta_o + \beta - 2\alpha + 2\gamma,$$

where δ_o is the site’s zenith declination, α is the inclination of the support of the mirror, β is the angle of the parabolic dish beam with respect to the zenith and γ is the mirror’s tilt angle. The radiometer beam is formed by a cooled corrugated feed horn that underilluminates an ambient-temperature 1.8 m paraboloid, which in turn illuminates the precessing mirror. This offset parabolic reflector with a corrugated feed has minimal blockage, approximately equal E/H -plane beam widths, and relatively low sidelobe response. These properties are ideal for CMB observations. All the beam-forming optics are inside a fixed aluminium ground screen. Figure 1 shows the optical and mechanical configuration of the instrument.

The spinning mirror is driven by an AC motor at a constant speed of ~ 60 rpm. The mirror has a tilting base that enables the elevation of the instrument to be changed. The optical set-up points north with a range of possible declinations between 10° and 60° . The spin axis of the mirror assembly has an optical encoder which generates one pulse per revolution to control the real speed and to serve as a physical direction reference for the instrument.

2.2 Receivers

The total-power receiver (see Figure 2) at the focal point of a paraboloidal antenna comprises a cryostat cooled to 20 K, which houses an HEMT amplifier (first amplification stage), a single feed horn and the calibration source. There is a second amplification stage at ambient temperature, together with a band splitter, filters and detectors before the voltage to frequency (VTF) converters. The sky signal enters the receiver through an 8 cm diameter and 3 mm thick polypropylene window. Two overlapping aluminium baffles define the entrance aperture. One is anchored to the ~ 80

Figure 1. *Top:* Scanning strategy of the experiment. *Bottom:* Mechanical and optical configuration of the experiment.

K stage, the other at ambient temperature. Strips of aluminized mylar electrically connect the top of the feed to the warm baffle and suppress RF interference.

The beam is formed by a conical corrugated scalar feed. This feed is matched with an electroformed adiabatic round-to-square transition to a semirigid waveguide. The signal is fed directly into one K-band Berkshire Technologies Inc. amplifiers (K-15.0-25H). This device has a 6 GHz bandwidth (~ 12.0 – 18.0 GHz) and a +28 dB (min) RF gain. The noise temperature across the bandwidth for this amplifier is 12 K (max), when cooled to ~ 20 K. The amplifier has isolators at the input and output to prevent reflections. The amplified signal is connected to the back-end amplifiers (warm stage) through stainless-steel waveguides. The RF signal is split into three 1 GHz bands centred at 12.5, 14.5 and 16.5 GHz (hereafter we will refer to these sub-bands as the 13, 15 and 17 GHz channels). Figure 3 shows the spectral response of these three channels.

The cryogenic components are cooled by an APD Joule–Thomson refrigerator. All mechanical and electrical connections from the cold stage to ambient temperature are thermally anchored to the refrigerator ~ 80 K stage. With an APD compressor, the cold stage runs at ~ 20 K. The amplifiers and the corrugated horn are anchored to this stage. The room-temperature receiver box is rigidly mounted on the cryostat base. The diode sensitivity and amplifier gain are a function of temperature and accordingly the temperature of the receiver enclosure is regulated for field operation. The RF components are fitted with insulation to prevent convective cooling and are thermally anchored to a common aluminium mounting plate.

A thermally controlled noise diode radiates a calibration signal of ~ 2.0 K directly into the corrugated horn for 1 second before and after each 30 seconds of observations. These calibration data are then used to correct the gain fluctuations of the amplifiers. The calibration data are then

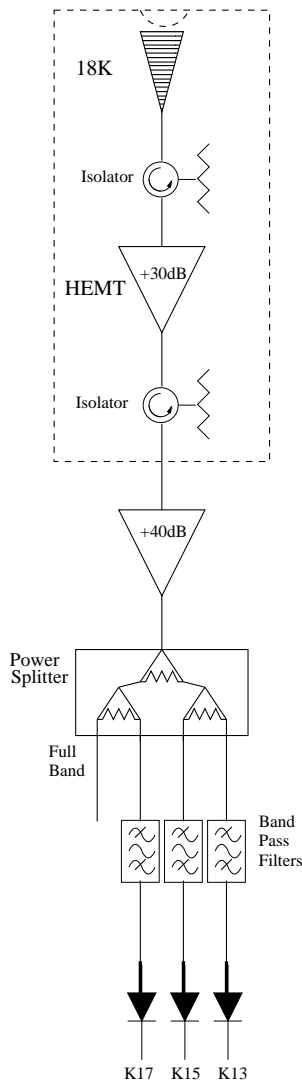


Figure 2. COSMO15 receiver layout. Radiation enters through the vacuum window and is collected by a cooled corrugated feed. The signal is amplified by a broad-band HEMT amplifier ($\Delta\nu = 6$ GHz), separated into three frequency bands and square-law detectors.

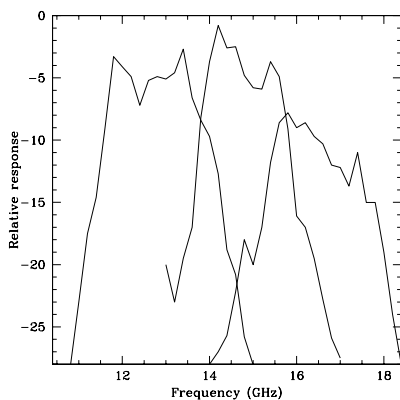


Figure 3. Relative spectral responses of the 13, 15 and 17 GHz channels.

obtained by subtracting the signals with *cal-off* from the those with *cal-on*.

2.3 Data acquisition system

The output voltage signal from the three channel detectors are read with VTF converters which are connected to the detectors with shielded pairs to minimize earthing problems. Along with the receiver channels, the spin encoder is read once per revolution, giving a total of four digital signals fed into the VTF converters. The output signals from the VTF converters are read by a counter card in a PC computer situated in an adjacent building. This computer also controls the square wave used to drive the calibration diode on and off. The computer is connected to the VTF converters and the calibration diode via a fast link which consists of two TTL-ECL converters, one at each of the connecting points.

The data are sampled each $4000 \mu\text{s}$ with a blanking time (no recording) of $400 \mu\text{s}$. This is equivalent to have three samples per beam and a total of ~ 220 samples per turn of the mirror. The computer temporally stores 30 seconds of data (about 30 turns of the mirror). For each turn of the mirror a lock-in at multiples of the spin cycle is performed by decomposition into a Fourier series. The first 106 Fourier coefficients (harmonics hereafter) which correspond to 212 samples per turn are kept and stacked across the 30 second period. The stacked harmonics are then stored in a FITS file. This procedure does not only saves hard-disk space on the PC but also accelerates the data reduction, because the 212 samples represent fixed positions on the sky. This is possible because the change in RA caused by the earth rotation in 30 seconds $\sim 0^\circ.12$ is negligible with respect to the beam-width $\sim 1^\circ$.

3 OBSERVATIONS, DATA PROCESSING AND ASTRONOMICAL CALIBRATION

The instrument is installed at the Teide Observatory, which has been shown to be a good site for centimetre and millimetre CMB observations (Davies et al. 1996; Dicker et al. 1999). The instrument started operation on 1999 September 1 and has remained operational until 2000 September, with interruptions due to instrumental tests, adverse atmospheric conditions and technical failure. During this period we have observed three overlapping regions of the sky between 16° and 46° in declination. About 100 days of data were obtained, of which we have selected the best ~ 50 days in terms of atmospheric quality in order to generate a first set of maps. Most of the observation time was devoted to the two high declination regions $22^\circ - 46^\circ$ while at the low declination region $16^\circ - 36^\circ$ only 8 days of good observations were obtained.

3.1 Scan reconstruction, offset removal and map making

The individual scans are reconstructed from the stored harmonics via an FFT using IDL routines on a workstation. A scan consists of 212 points which represent fixed positions in hour angle (HA) and declination (DEC). The top diagram of Figure 4 represents a typical COSMOSOMAS

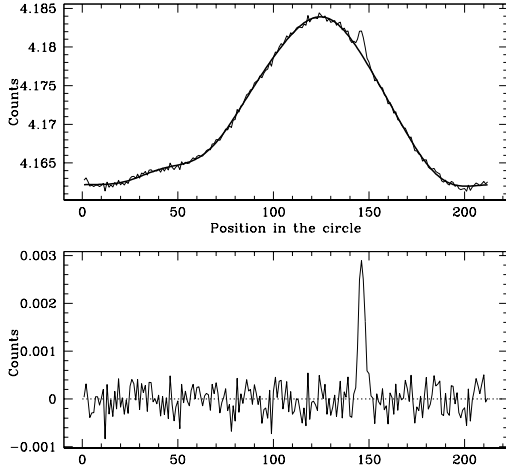


Figure 4. Tau A crossing in a 30 sec scan. The modulation due to atmospheric and ground spillover contribution is corrected by fitting a sine-cosine function to the cycle (heavy line).

scan containing the point source Tau A. The main modulation observed is due mostly to the change in air masses and ground pickup as the instrument scans a circle on the sky. To reduce the dominant ground pick-up effect, we have covered the ground surrounding the instrument with aluminum plates and have increased the size of the spinning mirror that is currently heavily under-illuminated. Data affected by the Sun or Moon were removed.

To remove these spurious signals, we use Fourier series to subtract low Fourier components from the data. Firstly, we reduce the effect of changes in the gain of the instrument by dividing the data by the calibration signal. Secondly, we fit each of the scans to a Fourier series of 11 coefficients, which means five sines and cosines plus a total power level and subtract the fit from the data. Therefore, angular scales larger than 5 degrees are removed from the data, limiting the angular resolution range to $1^\circ - 5^\circ$, but most of the atmospheric contribution is also removed. This procedure works very well but needs to be repeated iteratively so that strong astronomical features such as the Galaxy are preserved and no extra baseline is introduced around them. At each fitting step a re-weighting of the data is performed so that data three sigma away from the best fit are zero-weighted for the next step. After three or four iterations, contributions from strong astronomical sources are weighted to zero and the atmospheric shape is accurately reproduced by the fit. The upper diagram of Figure 4 also displays such a fit to the scan, while the lower diagram shows the residuals after baseline subtraction.

Long drift baselines possibly due to changes in atmospheric conditions throughout the day are still present in the data. To reduce these, we perform a second fit to the data. Each of the positions in the scans throughout the day are fitted to Fourier series of seven coefficients and the fit is subtracted from the data. This fitting procedure only removes from the data features at angular scales larger than 20° and therefore it does not affect the $1^\circ - 5^\circ$ structure we are able to observe. Note that in this case we also perform

Table 1. Antenna temperatures for calibration sources

ν (GHz)	Tau A (mK)	Cyg A (mK)
13.0	246.7	52.6
15.0	190.0	36.2
17.0	173.3	29.1

an iterative procedure to reduce the effect of Galaxy on the baseline fit. Once the fitting procedure is finished the clean scans are saved as IDL FITS files along with the Julian date.

For each clean scan we reproduce the instrumental pointing on the sky and derive out RA and DEC for each position in the scan. A simple projection scheme is used so that each RA and DEC position is converted into pixel positions in the map. For each pixel in the map we calculate an average contribution from all the scan positions lying within that pixel. The mean temperature value and dispersion are calculated for each pixel. Points within the pixel three sigma away from the mean value are excluded from the final result and the map-making process is repeated iteratively. The final map is composed of a mean value map, an error map and a number of points per pixel map that are stored in a single IDL FITS file. Pixels of $1/3 \times 1/3$ degrees in RA and DEC are used because they sample properly the beam response and minimize the noise contribution per beam area.

The first region observed covers the range from 16° to 36° in declination and the second one covers the range from 25° to 45° . Both have complete RA coverage. The latter region is of special interest because it overlaps that observed by the radiometers of the Tenerife Experiment (Gutiérrez et al. 2000) and the 33 GHz interferometer (Dicker et al. 1999, Harrison et al. 2000) and will allow for a future comparison.

3.2 Astronomical calibration

Our primary calibration sources are the supernova remnant Tau A for the low declination observations and Cyg A for the higher declinations. We measure the beam of the instrument using these two sources. Each beam was fitted as an elliptical Gaussian to the main lobe. The sidelobes are 40 dB below the main beam. Figure 5 shows the observations of Tau A, and the two-dimensional fit of the beam. From this analysis we conclude that the main beam is described by a circular Gaussian with FWHMs of $1.08^\circ \pm 0.07^\circ$ at 13 GHz, $1.04^\circ \pm 0.07^\circ$ at 15 GHz and $0.94^\circ \pm 0.05^\circ$ at 17 GHz. The flux densities were estimated from the compilation by Baars et al. (1977). The resulting spectral fit for Tau A is $\log(S_\nu/\text{Jy}) = (3.915 \pm 0.031) - (0.299 \pm 0.009) \log(\nu/\text{MHz})$ in the 1 to 35 GHz range and for Cyg A is $\log(S_\nu/\text{Jy}) = (7.161 \pm 0.053) - (1.244 \pm 0.014) \log(\nu/\text{MHz})$ in the 2 to 31 GHz frequency range. Using the beam parameters determined from these sources, we predict the antenna temperature for Tau A and Cyg A, which are listed in Table 1 and these values are used for the determination of the temperature scale.

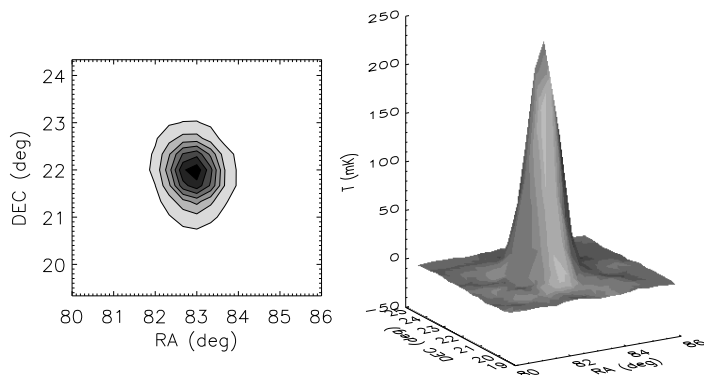


Figure 5. The reconstruction of Tau A.

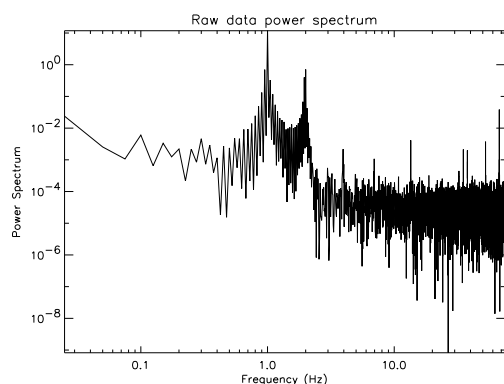


Figure 6. Power spectra of the raw data showing the $1/f$ noise.

4 INSTRUMENT PERFORMANCE

Figure 6 shows the power spectrum of a two-hour period of raw data taken on 1999 November 22. We can observe three main features in the plot. The $1/f$ noise component is seen at low frequencies (< 0.3 Hz) and the Gaussian noise at high frequencies (> 4 Hz). The knee frequency, defined as the frequency at which the Gaussian and $1/f$ noise have equal power, is ~ 2.7 Hz. We also observe an intermediate regime (0.5 - 2.5 Hz) which correspond to the atmospheric and ground pickup contributions which are superimposed to the $1/f$ noise.

The peaks at 1 Hz and 2 Hz are caused by the variation of the atmospheric emission and the ground pickup with zenith angle for a turn of the mirror. We also observe peaks at 3, 4 and 8 Hz which are the high frequency components of this variation. These features are synchronous with the spinning frequency (1 Hz) of the mirror and stable between scans. Therefore they cause the modulation discussed in section 3.1. The dispersion observed between the 1 and 2 Hz peaks is mainly due to changes in the atmospheric con-

Table 2. Theoretical sensitivity of COSMO15

Frequency (GHz)	T_{sys} (K)	ΔT_{pixel} (mK)
13	38.5	1.18
15	33.5	1.17
17	37.9	1.18

Table 3. Calibration and efficiency of each channel

Channel (GHz)	CAL_m (mK)	CAL_a (mK)	Efficiency
13	8150	12036	68 %
15	7770	11019	70 %
17	2920	3989	73 %

ditions. In the case of a non-spinning instrument this would show up as a noisy bump in the spectrum.

Finally, a 50 Hz peak is present and it is due to contamination from the mains. Extreme care has been taken to reduce its contribution to a minimum; however complete elimination has not been achieved. Nevertheless the 50Hz contribution is filtered out by software.

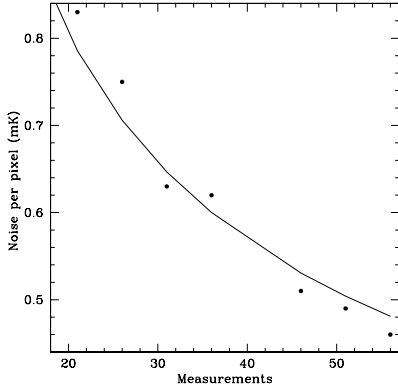
The sensitivity of the instrument depends basically on the efficiency of the optical configuration and the system temperature. We determined the system temperature using standard hot and cold load calibration procedures. We used a room-temperature absorber as a hot load and the sky as a cold load and measured the output power with a power meter connected just before each channel detector. Table 2 contains the system temperature and the expected r.m.s. noise per pixel ~ 1.2 mK in the 13 GHz, 15 GHz and 17 GHz channels for a typical day of observation (2000 June 11).

The optical efficiency was estimated as follows. COSMO15 has a calibration diode to monitor the receiver fluctuations. The temperature of this diode at each COSMO15 frequency can be measured if the system temperature is known by applying a hot and cold load method to diode on and off. The calibration factor measured this way does not depend on the optical system of the telescope. However, the astronomical calibration factor does depend on the characteristics of the whole system. One can compare both factors and deduce the efficiency of the system. For a 100 % efficient system the values should be similar to within the noise. Otherwise, the astronomical calibration factor should be larger (i.e. the observed signal smaller). The ratio CAL_m/CAL_a where CAL_m is the measured calibration factor and CAL_a is the astronomical calibration factor, is a direct measurement of the efficiency of the system. Table 3 shows the measured and astronomical calibration factor and the efficiency at the 13, 15 and 17 GHz channels for the data taken on 2000 June 11.

We have repeated the above calculations on indepen-

Table 4. Sensitivities in one day of observation

Channel (GHz)	$\Delta T_{\text{pixel}}^{\text{scans}}$ (mK)	$\Delta T_{\text{pixel}}^{\text{map}}$ (mK)
13	2.56	2.80
15	2.43	2.80
17	3.72	4.00

**Figure 7.** The noise as a function of integration time.

dent days and found efficiency factors of 68, 69, and 74 % at 13, 15 and 17 GHz respectively. The noise figures calculated from the maps are larger than expected from the system temperature of the instrument but not fully compatible with the efficiency factors measured. Two extra factors should be taken into account: error in the mapping process (mainly arising from difficulties in the atmospheric destriping) and extra noise coming from other unidentified contributions. Comparing the expected noise and the noise calculated from single scans to the noise found in the maps, we find that at 13 and 15 GHz the error in the mapping process dominates. Table 4 shows the noise estimates calculated from individual scans and from the maps at 13, 15 and 17 GHz for 2000 June 11.

We have checked for the presence of systematic residuals in the daily data and conclude that after subtraction of the above mentioned offsets the daily data are dominated by random noise. The noise per beam area σ in the stacked maps is reduced as $\frac{1}{\sqrt{N}}$ where N is the number of stacked maps (Figure 7).

We conclude that most of the increase of the noise in the maps at 13 and 15 GHz compared with the expected noise from the system temperature is due to the inefficiency of the optical system. However, at 17 GHz we have found another cause for the extra noise. Most of the microwave components of the system have a cut-off in their spectral behaviour for frequencies higher than 17 GHz, which could produce a narrower effective bandwidth in the 17 GHz channel.

Figure 8. The stacked COSMOSOMAS maps at 13, 15 and 17 GHz.

5 THE FIRST COSMOSOMAS MAPS

The final maps at each frequency resulting from observations conducted up to 2000 June are presented in Figure 8. These comprise the combination of 56, 49 and 46 good days of data at 13, 15 and 17 GHz, respectively, obtained at the low- and the high-declination set-up. The total region observed comprises a full band in RA and from 16° to 46° in declination, hence covering about 9000 square degrees. The noise levels per beam area are 140, 150 and $250 \mu\text{K}$ at 13, 15 and 17 GHz respectively. These sensitivities correspond to the high galactic latitude part of the maps. The lower declinations are noisier because the data set was smaller than at high declinations. Although some residual rings due to the $1/f$ noise were evident in the daily maps (see previous section), these have cleared up in the combined maps.

The Galactic plane crossings, the calibration sources Tau A and Cyg A, and some of the strongest radio sources can be clearly seen. Besides the principal calibrators, Tau A and Cyg A, the expected amplitude of the strongest radio sources have been estimated from the measurements by the Michigan monitoring programme (Aller & Aller, private communication); these have been complemented by the Kühr et al. (1981) and Green Bank (Condon, Broderick & Seielstad 1989) catalogues of discrete radio sources. Away from the Galactic plane the main contributors are the radio sources 3C 84, 3C 345, 4C 39.25 and 3C 286. In Table 5 we present the temperatures measured in the stacked maps for these sources which are in good agreement with expectations from the above mentioned catalogues. The uncertainties in the estimation of these amplitudes are $\sim 450 \mu\text{K}$ at 13 and 15 GHz, and $\sim 800 \mu\text{K}$ at 17 GHz. Although there are evidence of the presence of the 3C 286 source in the map at 17

Table 5. Temperatures measured for the strongest radio sources ($|b| \geq 10$ degrees) in the COSMOSOMAS maps

Name	α (J2000)	δ (J2000)	T_{13}	T_{15} (mK)	T_{17}
3C 84	03 ^h 19 ^m 48 ^s	+41°30′42″	9.4	7.2	5.5
4C 39.25	09 ^h 27 ^m 03 ^s	+39°02′21″	4.5	3.6	3.2
3C 286	13 ^h 31 ^m 09 ^s	+30°31′48″	1.5	1.4	≤ 1.6
3C345	16 ^h 42 ^m 59 ^s	+39°48′37″	4.9	4.1	3.3

Figure 9. A comparison of the Cyg X region in the COSMOSOMAS maps and existing maps at 420 and 1420 MHz.

GHz, due to its small amplitude as compared with the noise in this map, we decided to quote a 95 % upper limit.

In the region of the Galactic plane several point-like and extended sources are detected at the three frequencies. Good agreement between the positions and fluxes of these sources have been found when comparing our data with the low-frequency maps at 408 MHz (Haslam et al. (1982) and 1420 MHz (Reich 1982; Reich & Reich 1986). This is illustrated in Fig. 9, where we display these surveys and our data in the region of Cyg X. Cyg A is the source on the left of the plot, while most of the other structure corresponds to the Cyg X complex. A detailed analysis of the structure detected in our maps and a comparison between these datasets and the Galactic plane survey at 8.35 and 14.35 GHz (Langston et al. 2000) will be presented in a forthcoming paper.

6 CONCLUSIONS

1) We have presented a new ground-based CMB experiment working at 13, 15 and 17 GHz and an angular resolution of 1 degree based on a circular scanning strategy. The perfor-

mance of the system and the reliability of the data obtained during the first months of commissioning and operation have been discussed. We have demonstrated the possibility of removing the atmospheric and differential ground pickup effectively by the use of simple techniques that take into account the variation on angular and time scales of such components. Daily maps covering 6000 square degrees of the sky are routinely obtained with sensitivities of $\sim 800 \mu\text{K}$ per beam area (FWHM $\sim 1^\circ$) at each frequency.

2) Observations at two different elevations have been performed providing a stacked map of 9000 square degrees at 13, 15 and 17 GHz with mean sensitivities of 140, 150 and 250 μK per beam area respectively. These stacked maps show no evidence of systematics or striping due to $1/f$ noise or residual atmospheric fluctuations.

3) The strongest radio sources at high Galactic latitudes have been detected at the levels expected and the structure seen in the Galactic plane is in good agreement with the low-frequency surveys at 408 and 1420 MHz.

4) Several improvements of the system have been discussed. They include updating of the filters and optics, which will improve the sensitivity of the daily data by a factor 2 and will allow a sensitivity of 30 μK to be achieved after two years of operation.

ACKNOWLEDGEMENTS

We wish to thank especially R. D. Davies and are also grateful to R. J. Davis, J. Delabrouille, S. Hidalgo, J. Kaplan, P. Leahy, L. Piccirillo, B. Revenu and F. Villa for useful suggestions on this experiment. We are indebted to the mechanical and electronic personnel of the IAC working at Teide Observatory, who have collaborated in the installation and operation of the experiment. J. Gallegos was supported by an AECI PhD grant and J. Macías-Pérez acknowledges a PPARC-(IAC) research studentship. The COSMOSOMAS experiment is supported by the Spanish grants DGES PB95-1132-C02-01 and PB 98-0531-C02-02.

REFERENCES

- Baars J. W. M., Genzel R., Pauliny-Toth I. I. K., Witzel A., 1977, *A&A*, 61, 99
- Bennett C. L. et al., 1996, *ApJ*, 464, L1
- Condon J. J., Broderick, J. J., Seielstad, G. A., 1989, *AJ*, 97, 1064
- de Bernardis P. et al., 2000, *Nat*, 404, 955
- de Oliveira-Costa A. et al., 1999, *ApJ*, 527, L9
- de Oliveira-Costa A. et al., 2001, *astro-ph/0010527*
- Dicker S. R. et al., 1999, *MNRAS*, 309, 750
- Davies R. D. et al., 1996, *MNRAS*, 278, 883
- Draine B. T., Lazarian A., 1998, *ApJ*, 494, L19
- Gallegos J. E., Gutierrez, C. M., Rebolo, R., Hoyland, R. J., & Watson, R. A. 2000, *Proceedings of the 19th Texas Symposium on Relativistic Astrophysics and Cosmology*, . Eds.: E. Aubourg, T. Montmerle, J. Paul, & P. Peter. NH
- Gutiérrez C. M., Rebolo R., Watson R. A., Davies R. D., Jones A. W., Lasenby A. N., 2000, *ApJ*, 529, 47
- Halverson, N. W. et al. *astro-ph/0104489*
- Hanany, S. et al., 2000, *ApJ*, 545, L5
- Harrison D. L. et al., 2000, *MNRAS*, 316, 24
- Haslam C. G. T., Salter C. J., Stoffel H., Wilson W. E., 1982, *A&AS*, 47, 1

- Kogut A. et al., 1996a, ApJ, 460, 1
Kogut A. et al., 1996b, ApJ, 464, L5
Kuhr H., Witzel A., Pauliny-Toth L. I. K., Nauber U., 1981,
A&AS, 45, 367
Langston G., Minter A., D'Addario L., Eberhardt K., Koshi K.,
Zuber J., 2000, AJ, 119, 280
Mauskopf, P. D. et al. 2000, ApJ, 536, L59
Mukherjee P., Hobson M. P., Lasenby A. N. 2001, MNRAS, 320,
224
Reich W., 1982, A&AS, 48, 219
Reich P., Reich, W., 1986, A&AS, 63, 205

This paper has been produced using the Royal Astronomical
Society/Blackwell Science L^AT_EX style file.

This figure "f1.jpeg" is available in "jpeg" format from:

<http://arxiv.org/ps/astro-ph/0108020v1>

This figure "f8.jpeg" is available in "jpeg" format from:

<http://arxiv.org/ps/astro-ph/0108020v1>

This figure "f9.jpeg" is available in "jpeg" format from:

<http://arxiv.org/ps/astro-ph/0108020v1>